2018-03-15

# The distribution of lead concentrations and isotope compositions in the eastern Tropical Atlantic Ocean

Bridgestock, L



10.1016/j.gca.2018.01.018
GEOCHIMICA ET COSMOCHIMICA ACTA
Elsevier BV

Available online at www.sciencedirect.com

ScienceDirect

Geochimica et Cosmochimica Acta 225 (2018) 36–51

Geochimica et Cosmochimica Acta

www.elsevier.com/locate/gca

# The distribution of lead concentrations and isotope compositions in the eastern Tropical Atlantic Ocean

Luke Bridgestock [a,*], Mark Rehkämper [a], Tina van de Flierdt [a], Maxence Paul [a], Angela Milne [b], Maeve C. Lohan [c], Eric P. Achterberg [d]

[a] Department of Earth Science and Engineering, Imperial College London, London SW7 2AZ, UK
[b] School of Geography, Earth and Environmental Sciences, University of Plymouth, Plymouth PL4 8AA, UK
[c] Ocean and Earth Sciences, National Oceanography Centre Southampton, University of Southampton, Southampton SO14 3ZH, UK
[d] GEOMARHelmholtz Centre for Ocean Research, Kiel 24148, Germany

Received 17 October 2017; accepted in revised form 14 January 2018; available online 2 February 2018

## Abstract

Anthropogenic emissions have dominated marine Pb sources during the past century. Here we present Pb concentrations and isotope compositions for ocean depth profiles collected in the eastern Tropical Atlantic Ocean (GEOTRACES section GA06), to trace the transfer of anthropogenic Pb into the ocean interior. Variations in Pb concentration and isotope composition were associated with changes in hydrography. Water masses ventilated in the southern hemisphere generally featured lower $^{206}Pb/^{207}Pb$ and $^{208}Pb/^{207}Pb$ ratios than those ventilated in the northern hemisphere, in accordance with Pb isotope data of historic anthropogenic Pb emissions. The distributions of Pb concentrations and isotope compositions in northern sourced waters were consistent with differences in their ventilation timescales. For example, a Pb concentration maximum at intermediate depth (600–900 m, 35 pmol $kg^{-1}$) in waters sourced from the Irminger/Labrador Seas, is associated with Pb isotope compositions ($^{206}Pb/^{207}Pb = 1.1818–1.1824$, $^{208}Pb/^{207}Pb = 2.4472–2.4483$) indicative of northern hemispheric emissions during the 1950s and 1960s close to peak leaded petrol usage, and a transit time of ~50–60 years. In contrast, North Atlantic Deep Water (2000–4000 m water depth) featured lower Pb concentrations and isotope compositions ($^{206}Pb/^{207}Pb = 1.1762–1.1842$, $^{208}Pb/^{207}Pb = 2.4482–2.4545$) indicative of northern hemispheric emissions during the 1910s and 1930s and a transit time of ~80–100 years. This supports the notion that transient anthropogenic Pb inputs are predominantly transferred into the ocean interior by water mass transport. However, the interpretation of Pb concentration and isotope composition distributions in terms of ventilation timescales and pathways is complicated by (1) the chemical reactivity of Pb in the ocean, and (2) mixing of waters ventilated during different time periods. The complex effects of water mass mixing on Pb distributions is particularly apparent in seawater in the Tropical Atlantic Ocean which is ventilated from the southern hemisphere. In particular, South Atlantic Central Water and Antarctic Intermediate Water were dominated by anthropogenic Pb emitted during the last 50–100 years, despite estimates of much older average ventilation ages in this region.


*Keywords:* Anthropogenic Pb; Pb isotopes; Transient tracers; Ocean circulation

## 1. INTRODUCTION

During the past century, emissions from anthropogenic activities completely overwhelmed oceanic Pb inventories (Boyle et al., 2014). Of particular importance was the use

* Corresponding author at: Department of Earth Sciences, University of Oxford, Oxford OX1 3AN, UK.
*E-mail address:* luke.bridgestock@earth.ox.ac.uk (L. Bridgestock).

https://doi.org/10.1016/j.gca.2018.01.018
0016-7037/

of leaded petrol along with high temperature industrial processes such as metal smelting, coal combustion and waste incineration (Nriagu and Pacyna, 1988; Pacyna and Pacyna, 2001). Radiogenic Pb isotope compositions can provide insight into different sources of Pb to environmental systems. Notably, the isotope compositions of anthropogenic Pb emissions exhibit regional variations, reflecting the distinct Pb ores used to supply industrial and automotive activities in different economic areas (e.g. Bollhöfer and Rosman, 2001). This has resulted in spatial variability in the Pb isotope composition of ocean surface waters, which can be used to assess the relative contribution of anthropogenic and natural Pb inputs from different regional sources (Véron et al., 1994, 1998; Hamelin et al., 1997; Weiss et al., 2003; Noble et al., 2015; Paul et al., 2015a; Bridgestock et al., 2016).

Both the magnitude and isotope composition of anthropogenic Pb fluxes to the oceans have changed over time in response to known changes in anthropogenic activities (Boyle et al., 1986; Shen and Boyle, 1987; Véron et al., 1993; Wu and Boyle, 1997; Desenfant et al., 2006; Kelly et al., 2009). For example, since the 1920s Pb concentrations in North Atlantic surfaces waters have closely tracked the utilization of leaded petrol in the surrounding regions with a peak in the 1970s (Kelly et al., 2009). Accompanying temporal changes in the Pb isotope composition of Atlantic surface waters have been attributed to changes in the relative magnitude of Pb emissions from different areas (i.e. the US and Europe) as well as changes in the market share of particular Pb ores used within regions (Wu and Boyle, 1997; Véron et al., 1998; Hurst, 2002; Kelly et al., 2009).

These transient Pb inputs were subsequently transferred into the ocean interior predominantly by ocean circulation, as highlighted by time series measurements of Pb concentrations and isotope compositions throughout the water column at the Bermuda Time Series station conducted since 1979 (Chow and Patterson, 1966; Schaule and Patterson, 1983; Boyle et al., 1986; Shen and Boyle, 1988; Sherrell and Boyle, 1992; Véron et al., 1993, 1998; Lee et al., 2011; Boyle et al., 2012; Noble et al., 2015). The distribution of Pb concentrations and isotope compositions in the ocean interior can therefore provide insights into ventilation pathways and timescales, complementary to other anthropogenic transient tracers, such as CFCs, $SF_6$ and $^3H$ (e.g. Doney et al., 1997; Fine, 2011). However, Pb concentrations are not conserved during transport by ocean circulation due to removal by particle scavenging (Boyle et al., 1986; Shen and Boyle, 1988). Moreover, equilibrium exchange between adsorbed particulate and dissolved Pb may modify the isotope composition of seawater (Wu et al., 2010; Chen et al., 2016; Zurbrick et al., 2017). Finally, the mixing of waters ventilated at different times, featuring different Pb concentrations and isotope compositions, will complicate interpretations of ventilations pathways and timescales in a similar manner to the 'non-linear' mixing effects imposed on other transient tracers (e.g. Doney et al., 1997; Lee et al., 2017).

Unraveling the roles of transient Pb inputs, advection, mixing and particulate transport processes in setting the observed distributions of Pb in the ocean presents significant challenges. Efforts to improve the understanding of the processes controlling the cycling of Pb in the ocean are currently hindered by the sparse coverage of Pb concentration and isotope composition data, both spatially and temporally. In addition, the full potential of isotope variations to trace different sources of Pb to the ocean has yet to be realized. Studies tracing environmental Pb sources have typically focused on the relative abundances of $^{206}Pb$, $^{207}Pb$ and $^{208}Pb$, whilst neglecting the use of $^{204}Pb$ (e.g. Weiss et al., 2003). This is due to analytical difficulties in the precise determination of Pb isotope ratios featuring $^{204}Pb$, which has a low relative abundance of about 1% (Komárek et al., 2008). Hence, source apportionment is typically conducted using only two of three potential independently varying isotope ratios. Recent methodological developments now facilitate the precise measurement of Pb isotope ratios featuring $^{204}Pb$ in seawater, and thus the ability to fully utilize the potential of Pb isotope variations for source assessment (Paul et al., 2015b).

Here we present Pb concentrations and isotope compositions for seawater depth profiles and Pb concentrations of suspended particulate material collected in the eastern Tropical Atlantic Ocean (Fig. 1). Notably, the Pb isotope data include high precision results for ratios featuring $^{204}Pb$. These results are used to assess the controls on the distribution of Pb across a hydro-dynamically complex region of the ocean, transecting water masses ventilated in the northern and southern hemispheres and significant gradients in surface Pb inputs from natural and anthropogenic sources (Bridgestock et al., 2016).

## 2. SAMPLES AND ANALYTICAL TECHNIQUES

Samples were collected during the GEOTRACES GA06 section cruise on the RRS Discovery (D361; 7th February –

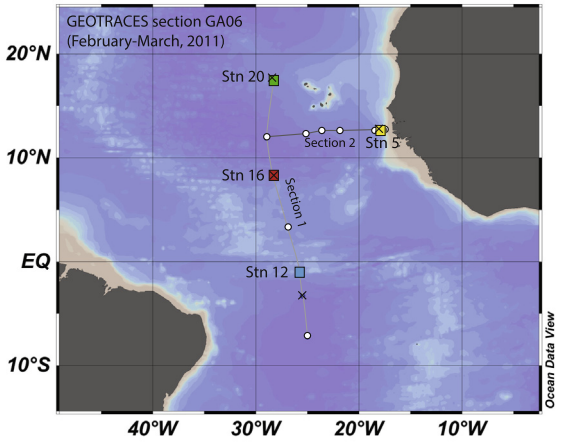


Fig. 1. Locations of samples collected during the GEOTRACES GA06 cruise in 2011. Colored squares show the location of depth profiles collected for Pb concentration and isotope composition analyses, crosses the locations of surface water samples collected close to each depth profile (Bridgestock et al., 2016), and open circles the location of depth profiles of particulate samples. Figure produced using Ocean Data View (Schlitzer, 2015). (For interpretation of the references to colour in this figure legend, the reader is referred to the web version of this article.)

19th March 2011). For Pb concentration and isotope composition analyses, seawater samples were collected throughout the water column at three stations describing an open ocean meridional transect, as well as one station on the continental shelf off the coast of Senegal (Fig. 1). Sample collection was conducted using a titanium rosette frame attached to a plasma rope, equipped with trace metal clean 10 L OTE (Ocean Technology Equipment) sampling bottles with external springs. In addition, data from (near) surface samples collected using a trace metal clean tow fish close to the locations of the depth profiles, are used to supplement this sample set (Bridgestock et al., 2016). Following seawater collection, samples were transferred into pre-cleaned 2 L low density polyethylene (LPDE, Nalgene) bottles inside a clean container and subsequently acidified to approximately pH 2 using quartz distilled 6 M HCl. No filtration was carried out.

Samples for particulate (>0.45 μm) elemental concentration analysis were collected throughout the water column at 14 stations that describe a zonal section extending from the continental shelf off the coast of Senegal, in addition to an open ocean meridional transect (Fig. 1). Within a clean container on board the ship, seawater was filtered from OTE sampling bottles under pressure (1.7 bar) of filtered nitrogen gas, onto acid-cleaned 25 mm Supor® polyethersulfone membrane disc filters (Pall, 0.45 μm). Samples were stored frozen at −20 °C, until shore-based analysis.

The Pb concentrations and isotope compositions of the unfiltered seawater samples were determined at Imperial College London following analytical protocols described by Paul et al. (2015b). Briefly, Pb concentrations were determined by isotope dilution, whereby a known quantity of Pb double spike solution ($^{207}$Pb–$^{204}$Pb) was equilibrated with about 50 ml of seawater. Following this, Pb was preconcentrated by $Mg(OH)_2$ co-precipitation and purified using a single stage anion exchange chromatography procedure, utilizing columns prepared from shrink-fit Teflon tubing, before analysis by thermal ionization mass spectrometry (TIMS; Thermo Scientific, TRITON instrument). Determined Pb concentrations were corrected for a procedural blank of $11.7 \pm 4.3$ pg (1sd, $n = 36$; Paul et al., 2015b) representing between 2.6 and 13% of the Pb processed in the samples. The Pb concentrations were measured in duplicate or triplicate for the majority of samples, especially those representing local maximums in the Pb concentration depth profiles, to check for artifacts caused by spurious high laboratory blanks. A single replicate measurement of one sample (station 12; 2999 m water depth) was discarded due to yielding a Pb concentrations 18.3 pmol kg$^{-1}$ higher that two other replicate analyses of this sample.

For isotopic analysis, Pb was separated from approximately 2 L of seawater by $Mg(OH)_2$ co-precipitation followed by a two stage anion exchange chromatography procedure, utilizing columns prepared from shrink-fit Teflon tubing. Measurements were conducted using TIMS, with instrumental mass bias corrected using a Pb double spike ($^{207}$Pb–$^{204}$Pb). Uncertainty in Pb concentrations (1 sd) and isotope compositions (2 sd) were assessed through replicate analyses of in-house seawater standards (Paul et al., 2015b). The accuracy of Pb concentration and isotope composition measurements by this technique were validated by analyses of GEOTRACES intercalibration samples GDI and GSI (Boyle et al., 2012) as reported by Paul et al. (2015b).

The particulate Pb concentrations were determined at the University of Plymouth. Particulate samples were subjected to the acid digestion method of Ohnemus et al. (2014) before analysis using ICP-MS (Thermo Fisher X series 2) equipped with a collision/reaction cell utilizing 7% H in He. The measured Pb concentrations were blank corrected with values obtained from replicate analyses of blank filters, which were acid washed and stored in the same manor as those used to collect the particulate samples. The efficiency of the digestion procedure was assessed using certified reference materials BCR-414 (Trace elements in plankton; Institute for Reference Materials and Measurements) and SO-2 (podzolic B horizon soil; Canadian CRM Project), with the determined Pb data in good agreement with the certified values (Supplementary Information; Table S1). Note that particulate Pb concentration data for the samples from the shallowest depths at stations 2, 12, 16, 18 and 20 have been previously published (Bridgestock et al., 2016).

## 3. HYDROGRAPHY

The water masses encountered during the meridional open ocean transect originate from the northern and southern hemisphere (Fig. 2). The upper 50–100 m ($\theta > 20$ °C) of the water column is composed of Tropical Surface Water (TSW) (Stramma and Schott, 1999). Embedded within TSW is a thin, high salinity layer (36–37) known as Subtropical Underwater (STUW) (Stramma and Schott, 1999). This water mass is formed by subduction in the Northern and Southern Subtropical gyres and was sampled for Pb concentration and isotope composition analysis at stations 20 and 12, at 86 and 64 m respectively (O'Connor et al., 2005). Below the TSW, the central waters ($\theta < 20$ °C $> \sigma_\theta = 27.1$) are dominated by South Atlantic Central Water (SACW) and North Atlantic Central Water (NACW), which are separated by the Cape Verde Frontal Zone at ~15°N (Emery and Meincke, 1986; Zenk et al., 1991).

Intermediate depth waters (500–1200 m, $\sigma_\theta = 27.1$–$27.6$) are composed of Antarctic Intermediate Water (AAIW) in the southern end of the transect and northern sourced waters from the Labrador Sea (LSW), Irminger Sea (ISW) and/or Mediterranean outflow (MOW) at the most northerly station 20 (Emery and Meincke, 1986; Jenkins et al., 2015). Samples collected along the $\sigma_\theta = 27.3$–$27.4$ neutral density horizons at about 750 m water depth, represent the core of AAIW in various stages of mixing with more saline northern sourced waters (Fig. 2).

Below about 1200 m ($\sigma_\theta = 27.6$) North Atlantic Deep Water (NADW) dominates the water column (Tsuchiya et al., 1992). The Mid Atlantic Ridge separates the bottom waters (below ~3500 m) in the western and eastern basins

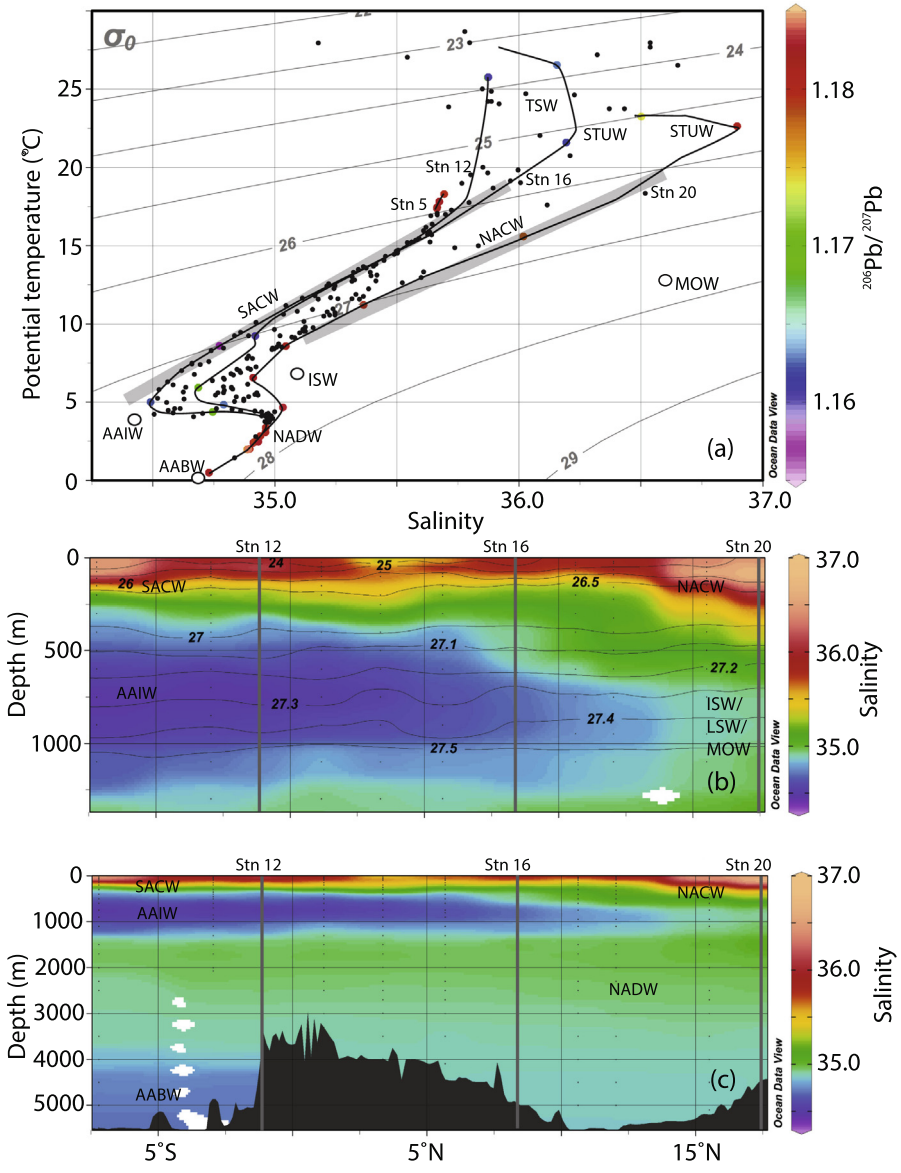


Fig. 2. Hydrography of the study area. Panel (a) displays potential temperature versus salinity, as determined during the GEOTRACES GA06 cruise. Solid black lines denote the stations sampled for Pb concentration and isotope composition analysis. Open circles show compositions of water mass endmembers (see text for abbreviations), with grey shaded regions marking the compositions of SACW and NACW (Emery and Meincke, 1986; Jenkins et al., 2015). Light grey lines denote potential density horizons ($\sigma_0$). The $^{206}Pb/^{207}Pb$ ratios for the analyzed samples are denoted by color of the points. Panel (b), section of salinity (colors) for shallow to intermediate depth waters (<1500 m), with positions of stations 20, 16 and 12 shown by the grey lines. Black contours show potential density horizons ($\sigma_0$). Panel (c) shows a section of salinity (colors) for the entire water column. The Figure was prepared using Ocean Data View (Schlitzer, 2015), and the hydrographic data are available as part of the GEOTRACES data product (Mawji et al., 2015). (For interpretation of the references to colour in this figure legend, the reader is referred to the web version of this article.)

(Schlitzer, 1987). At 1°S, the section crosses the Mid Atlantic Ridge into the western basin (Fig. 2), where a decrease in salinity and θ below about 4000 m indicates the presence of Antarctic Bottom Water (AABW), which was sampled for Pb concentration and isotope composition analysis at station 12, 4500 m water depth.

## 4. RESULTS

The $^{206}Pb/^{204}Pb$ and $^{206}Pb/^{207}Pb$ ratios displayed a strong correlation ($r^2 = 0.98$), with no independent variability from this relationship exceeding analytical uncertainty (Fig. 3a). In contrast, although correlated ($r^2 = 0.60$), the

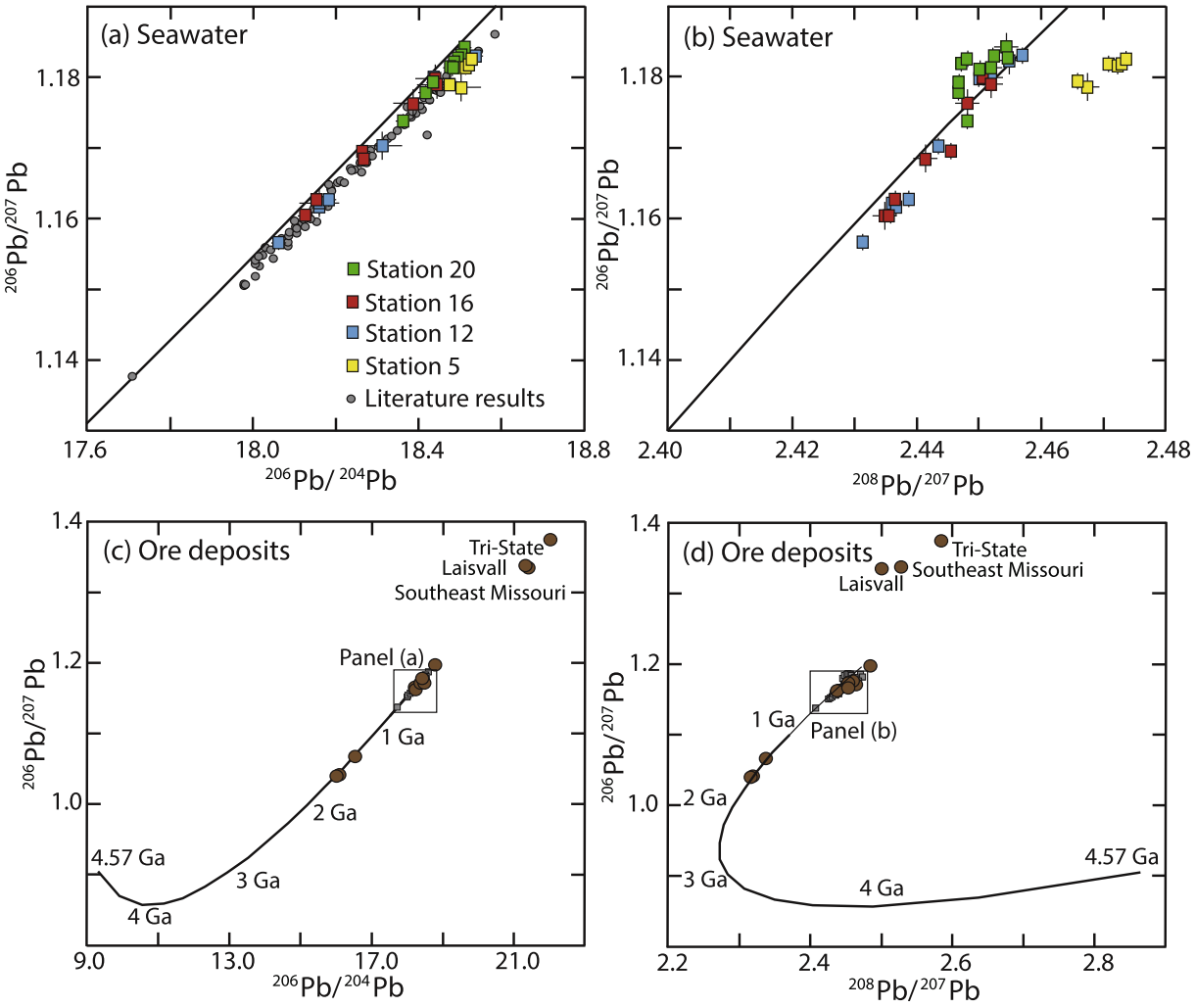


Fig. 3. Three isotope plots that display the Pb isotope systematics of the seawater samples and major Pb ore deposits that are important environmental Pb sources. Panels (a) and (b) display results for seawater from this investigation as well as published studies that feature high-precision $^{206}Pb/^{204}Pb$ data for seawater from the South Atlantic (Paul et al., 2015a,b), western Tropical Atlantic and aerosols from the eastern Tropical Atlantic (Bridgestock et al., 2016). Panels (c) and (d) display the Pb isotope compositions of major Pb ore deposits (Sangster et al., 2000). The black lines denote the evolution of the Pb isotope composition of the bulk continental crust over earth's history (Stacey & Kramers, 1975).

$^{206}Pb/^{207}Pb$ and $^{208}Pb/^{207}Pb$ ratios exhibited independent variability that exceeded analytical uncertainty and which can hence be used for source assessment (Fig. 3b). In the following, we therefore limit our description of the observed Pb isotope variations to the $^{206}Pb/^{207}Pb$ and $^{208}Pb/^{207}Pb$ ratios. The accuracy of the Pb concentration and isotope composition data is validated by comparison of results for station 20 to those obtained for depth profiles collected slightly further north during the GEOTRACES GA03 section cruise (Noble et al., 2015). These two datasets, obtained on waters collected on different cruises and analyzed using different analytical techniques, are in good agreement, with differences likely reflecting genuine spatial variability of these properties (Supplementary Information).

Lead concentrations for the unfiltered seawater (i.e. total dissolvable Pb) ranged from 7.5 to 43.2 pmol $kg^{-1}$ (Fig. 4a, Table 1). Particulate Pb concentrations (>0.45 μm) were typically <2 pmol $kg^{-1}$ in the open ocean depth profiles, but with some variability with higher concentrations of up to 4.2 pmol $kg^{-1}$ in the upper 500 m of the water column (Fig. 5; Supplementary Data). These values result in particulate Pb contributions of approximately 5–10% compared to the total dissolvable Pb content for the majority of the unfiltered samples (Table 1). Particulate Pb concentrations increased close to the continental margin, with highest values of 9.2–23.8 pmol $kg^{-1}$ determined at stations on the continental shelf. As such, close to 100% of the Pb contents of the unfiltered samples collected at station 5 were in particulate form (Figs. 1 and 4e). These samples also exhibited the highest $^{206}Pb/^{207}Pb$ and $^{208}Pb/^{207}Pb$ ratios of 1.1785–1.1824 and 2.4660–2.4737, respectively (Fig. 3b, Table 1). Elevated particulate Pb concentrations of up to approximately 5–6 pmol $kg^{-1}$ were also observed at various depths at stations situated on the continental slope (Fig. 5).

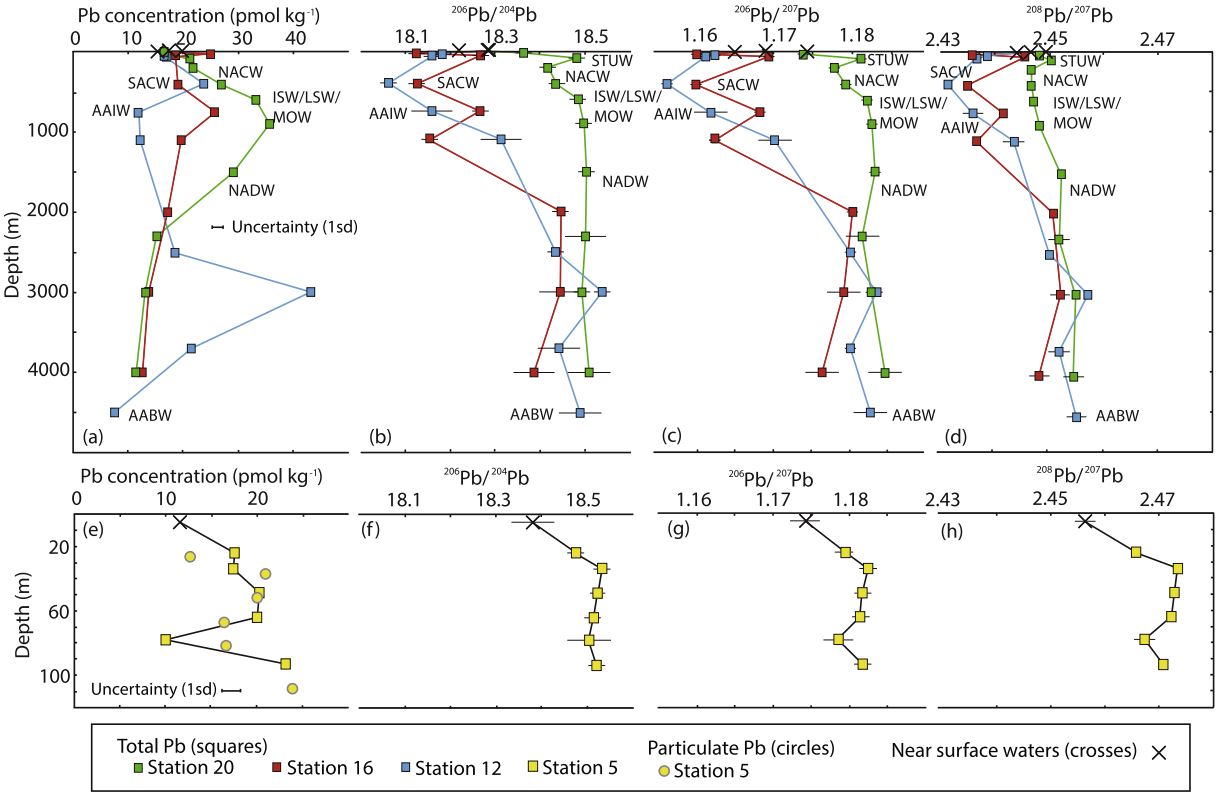


Fig. 4. Depth profiles of Pb concentrations and isotope compositions. Panels (a) to (d) display results for open ocean stations 12, 16 and 20. Panels (e) to (h) display results for station 5 on the continental shelf. Particulate Pb concentrations determined at station 5 are also shown in panel (e) as circles. Error bars for Pb concentrations (1sd) and Pb isotope ratios (2sd) were assessed through replicate analyses in-house seawater standards (Paul et al., 2015b). Corresponding water masses for the open ocean depth profiles are labeled; Subtropical Underwater (STUW), North Atlantic Central Water (NACW), South Atlantic Central Water (SACW), Irminger Sea Water (ISW), Labrador Sea Water (LSW), Mediterranean Outflow Water (MOW), Antarctic Intermediate Water (AAIW), North Atlantic Deep Water (NADW) and Antarctic Bottom Water (AABW).

Seawater samples collected within TSW (>50–100 m, θ > 20 °C), displayed relatively uniform Pb concentrations of 17.1–18.6 pmol $kg^{-1}$ for the open ocean stations except at station 16, which featured a near surface maximum (24.9 pmol $kg^{-1}$, depth 26 m; Fig. 4a, Table 1). This exceeds the Pb content of other samples from the mixed layer directly below (18.6 pmol $kg^{-1}$, depth 56 m) and of a sample collected at ~5 m water depth using a towed fish sampler close to the position of this station (15.8 pmol $kg^{-1}$; Bridgestock et al., 2016). The anomalously high Pb concentration of this sample is also associated with a pronounced positive excursion in $^{206}Pb/^{207}Pb$ and $^{208}Pb/^{207}Pb$ ratios compared to the samples at adjacent depth (Fig. 4). Such a high degree of variability in the mixed layer could potentially reflect contamination during collection and the results obtained for this sample should hence be treated with caution. However, this region does feature a complex, alternating zonal current system that could result in significant hydrographic changes over small length scales (tens of meters) in this depth range (e.g., Brandt et al., 2008), although no variations in temperature or salinity are observed that might support this. Apart from this, the observed spatial variability of Pb isotope compositions in TSW is consistent with gradients in atmospheric inputs, as discussed by Bridgestock et al. (2016).

At station 20, the occurrence of STUW was accompanied by an increase in Pb concentration to 21.5 pmol $kg^{-1}$, whilst at station 12 the Pb concentration of this water mass was indistinguishable to that of the overlying TSW (Fig. 4, Table 1). Furthermore, STUW sampled at station 20 featured a distinct Pb isotope composition relative to the underlying NACW and overlying TSW. This is consistent with the findings of Noble et al. (2015), who noted a distinct Pb isotope composition of this water mass, mapped along a high resolution quasi-zonal transect across the North Atlantic at ~20 to 40°N (GEOTRACES section GA03).

Below the TSW and STUW layers, variations in Pb concentrations and isotope compositions were associated with hydrographic changes, with water masses ventilated in the southern hemisphere generally featuring lower $^{206}Pb/^{207}Pb$ and $^{208}Pb/^{207}Pb$ than those ventilated in the northern hemisphere. The lowest $^{206}Pb/^{207}Pb$ and $^{208}Pb/^{207}Pb$ ratios, of 1.1566–1.1603 and 2.4313–2.4349, respectively, were found in SACW (~400 m depth, stations 12 & 16; Fig. 4, Table 1). At station 12, AAIW was sampled at 750 m water depth,

Table 1
Pb concentrations and isotope composition for seawater samples from four depth profiles collected in the eastern Tropical Atlantic during the GEOTRACES GA06 section cruise.

| Stn | Depth (m) | Total Pb concentration (pmol kg$^{-1}$) | n[a] | Particulate Pb concentration[b] (pmol kg$^{-1}$) | Particulate Pb contribution (%) | $^{206}Pb/^{204}Pb$ | $^{206}Pb/^{207}Pb$ | $^{208}Pb/^{207}Pb$ |
|---|---|---|---|---|---|---|---|---|
| 5 | 24 | 17.5 | 1 | 12.6 (26 m) | 73 | 18.4753 | 1.1794 | 2.4660 |
| | 34 | 17.4 | 1 | 20.9 (36 m) | 120 | 18.5320 | 1.1824 | 2.4737 |
| | 49 | 20.2 | 1 | 20.1 (51 m) | 99 | 18.5236 | 1.1818 | 2.4730 |
| | 64 | 20.0 | 2 | 16.4 (66 m) | 82 | 18.5143 | 1.1815 | 2.4724 |
| | 78* | 10.0 | 2 | 16.7 (80 m) | 166 | 18.5034 | 1.1785 | 2.4676 |
| | 93 | 23.1 | 2 | 23.8 (107 m) | 103 | 18.5220 | 1.1818 | 2.4709 |
| 12 | 45 | 16.3 | 1 | 0.9 (45 m) | 5 | 18.1826 | 1.1626 | 2.4388 |
| | 64 | 16.8 | 1 | 0.6 (60 m) | 4 | 18.1592 | 1.1615 | 2.4368 |
| | 395 | 23.7 | 1 | 1.9 (400 m) | 8 | 18.0622 | 1.1566 | 2.4313 |
| | 750* | 11.8 | 2 | 0.7 (750 m) | 6 | 18.1592 | 1.1621 | 2.4360 |
| | 1100* | 12.1 | 1 | 0.9 (1100 m) | 8 | 18.3123 | 1.1702 | 2.4436 |
| | 2500 | 18.4 | 2 | 1.2 (2500 m) | 6 | 18.4343 | 1.1797 | 2.4500 |
| | 2999 | 43.2 | 2 | 1.6 (2999 m) | 4 | 18.5382 | 1.1829 | 2.4571 |
| | 3699* | 21.4 | 2 | 1.3 (3699 m) | 6 | 18.4419 | 1.1798 | 2.4519 |
| | 4498* | 7.5 | 1 | 1.8 (4498 m) | 24 | 18.4909 | 1.1823 | 2.4550 |
| 16 | 26 | 24.9 | 2 | 1.8 (25 m) | 7 | 18.1251 | 1.1604 | 2.4359 |
| | 56 | 18.6 | 2 | 2.0 (54 m) | 11 | 18.2667 | 1.1695 | 2.4456 |
| | 404 | 19.0 | 2 | 1.4 (400 m) | 7 | 18.1266 | 1.1603 | 2.4349 |
| | 750 | 25.7 | 1 | 1.9 (750 m) | 7 | 18.2683 | 1.1683 | 2.4415 |
| | 1099 | 19.5 | 1 | 1.9 (1099 m) | 10 | 18.1540 | 1.1626 | 2.4366 |
| | 1999 | 17.2 | 1 | 2.3 (1999 m) | 13 | 18.4451 | 1.1799 | 2.4508 |
| | 2999* | 13.6 | 1 | 1.5 (2999 m) | 11 | 18.4434 | 1.1789 | 2.4520 |
| | 3999* | 12.6 | 2 | 0.7 (3999 m) | 5 | 18.3874 | 1.1762 | 2.4482 |
| 20 | 26 | 17.1 | 1 | 1.3 (24 m) | 8 | 18.3636 | 1.1737 | 2.4481 |
| | 86 | 21.2 | 1 | 1.4 (83 m) | 7 | 18.4815 | 1.1811 | 2.4503 |
| | 200 | 21.7 | 1 | 2.1 (200 m) | 10 | 18.4172 | 1.1778 | 2.4468 |
| | 405 | 26.9 | 1 | 2.9 (400 m) | 11 | 18.4371 | 1.1792 | 2.4469 |
| | 600 | 33.2 | 2 | 1.6 (600 m) | 5 | 18.4868 | 1.1818 | 2.4472 |
| | 899 | 35.7 | 2 | 2.5 (899 m) | 7 | 18.4987 | 1.1824 | 2.4483 |
| | 1499 | 29.0 | 2 | 2.3 (1499 m) | 8 | 18.5040 | 1.1829 | 2.4523 |
| | 2300* | 15.0 | 2 | 0.9 (2300 m) | 6 | 18.5024 | 1.1813 | 2.4519 |
| | 3000 | 13.0 | 2 | 1.0 (3000 m) | 8 | 18.4948 | 1.1826 | 2.4548 |
| | 3999* | 11.3 | 2 | 1.3 (3999 m) | 12 | 18.5105 | 1.1841 | 2.4545 |

Station 5 was occupied on the 22nd February, 2011 at 12.36°N, 17.34°W. Station 12 was occupied on the 6th March, 2011 at 1.1°S, 25.36°W. Station 16 was occupied on the 10th March, 2011 at 8.20°N, 28.20°W. Station 20 was occupied on the 14th March, 2011 at 17.23°N, 28.23°W.

[a] Number of Pb concentration measurements conducted. Quoted Pb concentrations are the mean of the conducted analyses and were corrected for a Pb blank of 11.7 ± 4.3 pg (1sd, n = 36) (Paul et al., 2015b).

[b] Concentration of particulate Pb at a depth that is identical or similar to the depth at which the sample for the total Pb concentration and isotopic analyses was collected; the exact depth is given in brackets. The relative precision of the Pb isotope data is 1‰, 1‰ and 0.25‰ for the $^{206}Pb/^{204}Pb$, $^{206}Pb/^{207}Pb$ and $^{208}Pb/^{207}Pb$ ratios respectively, based on replicate analyses of in-house seawater standards (Paul et al., 2015b).

* Denotes samples for which the Pb isotope data were assigned a relative precision of 2.6‰, 1.7‰ and 0.8‰ for $^{206}Pb/^{204}Pb$, $^{206}Pb/^{207}Pb$ and $^{208}Pb/^{207}Pb$, respectively, based on replicate analyses of in-house seawater standards (Paul et al., 2015b), due to larger within-run errors as only small quantities of Pb (<3 ng) were available for analysis.

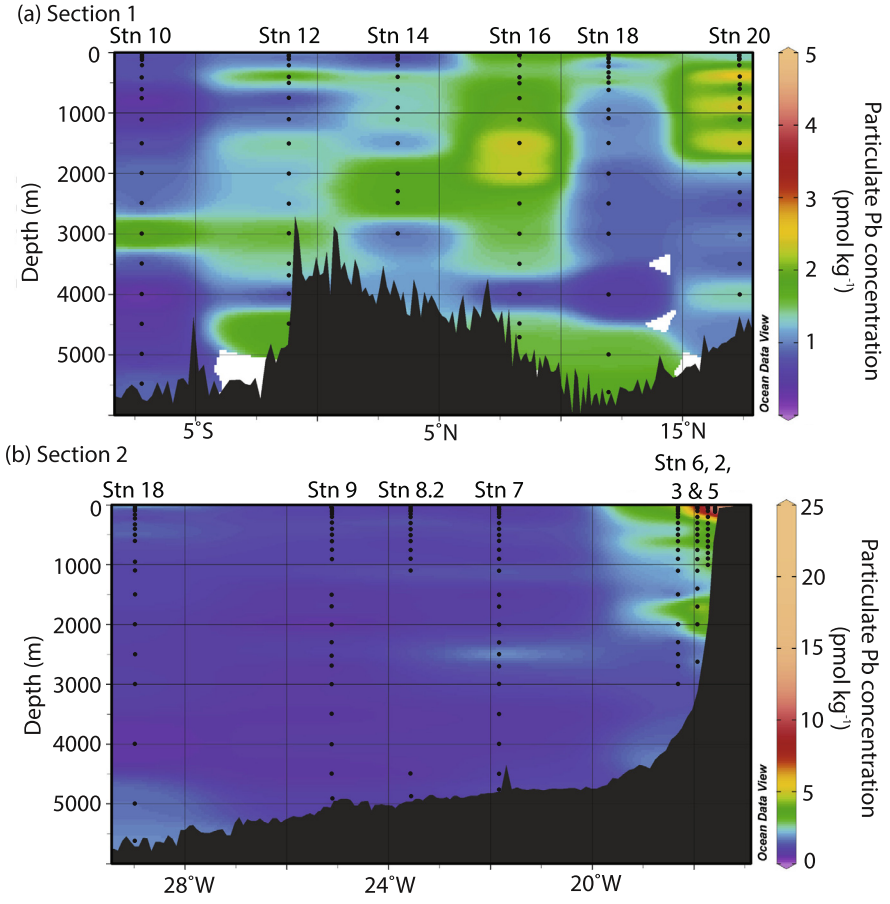


Fig. 5. The distribution of particulate Pb concentrations. Panel (a) displays results for the quasi-meridional Section 1, and panel (b) displays results for the zonal section 2 (Fig. 1). Note the large difference in the color scale between the two panels. The particulate Pb concentration data are presented the Supplementary Data.

featuring low Pb isotope ratios, with $^{206}Pb/^{207}Pb = 1.1621$ and $^{208}Pb/^{207}Pb = 2.4360$. These ratios are broadly consistent with those previously determined for AAIW in the Tropical and South Atlantic (Alleman et al., 2001; Paul et al., 2015b). In contrast, NACW sampled at station 20 between 200 and 405 m water depth featured higher $^{206}Pb/^{207}Pb$ (1.1778–1.1792) and $^{208}Pb/^{207}Pb$ (2.4468–2.4469) ratios. This isotope signature can be distinguished from the underlying intermediate water (600–900 m), which has slightly higher $^{208}Pb/^{207}Pb$ (2.4472–2.4483).

Lead concentrations increased to a relative maximum in central and intermediate water masses at all three open ocean stations (Fig. 4a). This maximum is particularly pronounced at the most northern station 20 extending down to at least 1500 m, with peak values of 33.2–35.7 pmol $kg^{-1}$ at 600–899 m corresponding to intermediate depth waters, LSW, ISW and/or MOW. At the most southern station 12, a maximum in Pb concentration of 23.7 pmol $kg^{-1}$ is reached at 395 m, corresponding to SACW. Below this, Pb concentrations drop to a minimum of 11.8 pmol $kg^{-1}$ at 750 m within the core of AAIW. Based on salinity, the sample situated at 750 m water depth from station 16, represents a mixture of AAIW (sampled at station 12), and the northern sourced waters, LSW, ISW and or MOW, (sampled at station 20; 600–900 m; Fig. 2). This sample exhibited a Pb concentration (25.7 pmol $kg^{-1}$) and isotope composition ($^{206}Pb/^{207}Pb = 1.1683$ and $^{208}Pb/^{207}Pb = 2.4415$) in between waters from comparable depths at station 12 and 20 (Fig. 4). Below this depth, at station 16 near the boundary between AAIW and NADW (1099 m, $\sigma_\theta = 27.5$) there was an observed decrease in $^{206}Pb/^{207}Pb$ (to 1.1626) and $^{208}Pb/^{207}Pb$ ratios (to 2.4366).

Between about 2000 and 4000 m, the NADW was characterized by a Pb isotope composition of $^{206}Pb/^{207}Pb = 1.1762–1.1841$ and $^{208}Pb/^{207}Pb = 2.4482–2.4500$, and Pb concentrations that steadily decreased with depth from about 17 pmol $kg^{-1}$ to 11 pmol $kg^{-1}$ (Fig. 4). A clear exception to this is the sample from 3000 m at station 12 that has an anomalously high Pb concentration of 43.2 pmol $kg^{-1}$, which is confirmed by repeat analyses (Table 1). The over and underlying samples at 2500 m and 3700 m, station 12, also showed slightly elevated Pb contents of 18.4 pmol $kg^{-1}$ and 21.4 pmol $kg^{-1}$ relative to those obtained from comparable depths at stations 16 and 20. Notably, these anomalous Pb concentrations were not associated with any deviation in Pb isotope composition.

The single seawater sample collected within the AABW (from station 12, 4498 m) featured the lowest Pb concentration of 7.5 pmol $kg^{-1}$ and had relatively high $^{206}Pb/^{207}Pb$ and $^{208}Pb/^{207}Pb$ ratios of 1.1823 and 2.4550 respectively, that resembled those of NADW (Fig. 4). These values are consistent with previously reported results for dilute AABW in the region (Alleman et al., 2001), and AABW sampled in the South Atlantic (Paul et al., 2015a). This sample also featured high particulate Pb contributions, amounting to about 24% of the total dissolvable Pb content of the unfiltered seawater (Table 1; Fig. 5). Such a high particulate Pb contribution reflects the low total dissolvable Pb content of these waters, rather than elevated particulate Pb concentrations relative to other samples from comparable depths (Table 1; Figs. 4 and 5).

## 5. DISCUSSION

### 5.1. Lead isotope systematics; the use of $^{206}Pb/^{204}Pb$ ratios for assessment of Pb sources

Fluxes of Pb to the oceans during the past century have been dominated by emissions from leaded petrol usage, with the Pb ultimately derived from a variety of ore deposits (Boyle et al., 2014). Since Pb ore minerals (i.e. galena) contain negligible quantities of the radioactive parent isotopes $^{238}U$, $^{235}U$ and $^{232}Th$ compared to Pb, the Pb isotope composition of these deposits ceases to evolve following their formation (Sangster et al., 2000). The primary control on the Pb isotope composition of such ore minerals is therefore their age, with a secondary control imposed by the Pb isotope evolution of the geological reservoir from which the Pb is derived (Sangster et al., 2000). The 12 most important ore deposits in terms of Pb production during the 20th century all lie on a linear trend in $^{206}Pb/^{204}Pb$ versus $^{206}Pb/^{207}Pb$ space (Fig. 3). Notably, these deposits lie on a linear section of the radiogenic growth curve for the isotopes $^{206}Pb$ and $^{207}Pb$, representing the temporal evolution of the Pb isotope composition of the bulk continental crust (Stacey and Kramers, 1975; Sangster et al., 2000). Exception to this are the US based deposits from the southeast Missouri and the Tri-State area, in addition to Laisvall in Sweden that exhibit anomalously radiogenic compositions, although they still plot along on the linear trend defined by the other deposits. Consequently, mixing of Pb derived from the large ore deposits shown in Fig. 3 will result in trends roughly parallel to this radiogenic growth curve in $^{206}Pb/^{204}Pb$ versus $^{206}Pb/^{207}Pb$ space, and these isotope ratios alone cannot be applied to distinguish Pb inputs from more than two of the deposits.

The Pb isotope systematics described above can account for the strong correlation observed between $^{206}Pb/^{204}Pb$ and $^{206}Pb/^{207}Pb$ ratios determined for the seawater samples presented here (Fig. 3a). Such a correlation is also observed for seawater from the South Atlantic (Paul et al., 2015a,b), western Tropical Atlantic and aerosols collected during the GEOTRACES GA06 section (Bridgestock et al., 2016). The Pb sources contributing to these samples are likely well mixed during anthropogenic processing and emission, followed by transport in the atmosphere and within the ocean. Such mixtures are likely to be dominated by Pb derived from the largest ore deposits in terms of Pb production, resulting in the observed Pb isotope systematics. This condition potentially also applies to environmental Pb reservoirs remote from original Pb sources, notably open ocean seawaters, which have integrated the Pb isotope composition of a large number of anthropogenic Pb sources.

These observations do not belie the use of ratios featuring $^{204}Pb$ altogether to provide unique information for discrimination of marine Pb sources. Certain Pb ore deposits exhibit Pb isotope compositions that do not fall on the radiogenic growth curve of the continental crust for the isotope ratios $^{206}Pb/^{204}Pb$ and $^{206}Pb/^{207}Pb$ (Sangster et al., 2000), however these variations are subtle, limited to within 10‰. In addition, natural Pb derived for the weathering of rocks may also originate from geological reservoirs that have experienced a time-integrated Pb isotope evolution that is distinct from the bulk continental crust. In such cases, the Pb will have an isotope composition that deviates from the observed correlation between $^{206}Pb/^{204}Pb$ and $^{206}Pb/^{207}Pb$ ratios (Fig. 3c), enabling unique insights into the Pb sources. However, because such reservoirs are expected to make only relatively minor contributions to Pb in the environment and ocean overall, they are likely to be only important close to the original sources, prior to significant mixing and dilution by Pb derived from the aforementioned large 'conformable' ore deposits.

The isotope compositions of the US based deposits from southeast Missouri and the Tri-State area, in addition to Laisvall, exhibit lower abundances of radiogenic $^{208}Pb$ relative to the average evolution of the continental crust (Fig. 3d). The Pb isotope signatures of the former two ore deposits were thereby clearly seen in the US and consequently northern hemispheric Pb emissions during the past century (Hurst, 2002). The variability observed in $^{208}Pb/^{207}Pb$ ratios relative to $^{206}Pb/^{207}Pb$ can therefore be used to distinguish past inputs from these prominent US ore deposits. Overall, the isotopic variations observed in seawater can be, to a first order, explained by mixing between Pb derived from a limited number of large ore deposits. Due to the isotope systematics of these deposits, the observed variations in $^{206}Pb/^{207}Pb$ and $^{208}Pb/^{207}Pb$ are sufficient to enable characterization of the Pb sources, at least for well-mixed environmental reservoirs such as open ocean seawater.

### 5.2. Sources of Pb to continental shelf waters

The Pb isotope compositions of samples from the depth profile collected on the continental shelf off the Senegalese coast at station 5 trend towards that of pre-anthropogenic Pb in a plot of $^{206}Pb/^{207}Pb$ versus $^{208}Pb/^{207}Pb$, whereby the Pb is predominately in the particulate form (Figs. 4e and 6). This likely reflects the importance of re-suspended shelf sediments, which feature a mixture of Pb derived from anthropogenic sources and detrital aluminosilicate minerals including North African mineral dust (Chow and Patterson, 1962; Abouchami and Zabel, 2003; Abouchami

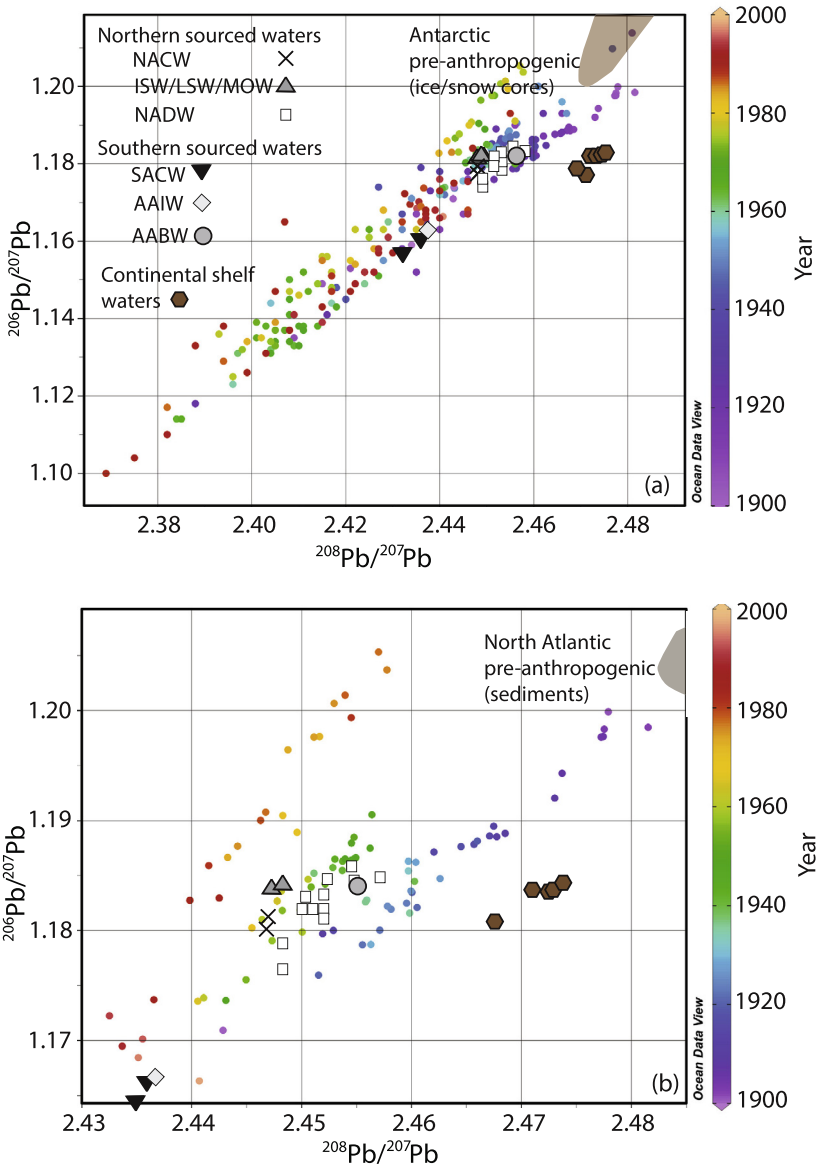


Fig. 6. Comparison of Pb isotope compositions determined for major water masses and the potential historic marine Pb sources to water mass formation sites. Panel (a) displays the temporal variation of Pb isotope ratios of anthropogenic inputs to Antarctic snow and ice cores during the last century (Planchon et al., 2003; Vallelonga et al., 2002; Van de Velde et al., 2005). Panel (b) displays the temporal variation of Pb isotope ratios of anthropogenic inputs to the western North Atlantic during the last century reconstructed using corals (Kelly et al., 2009). Also shown are the compositions of pre-anthropogenic Pb from Antarctic ice cores (panel (a); Vallelonga et al., 2002; Van de Velde et al., 2005) and North Atlantic Holocene sediments (panel (b); Chow and Patterson, 1962; Abouchami and Zabel, 2003). This Figure was prepared using Ocean Data View (Schlitzer, 2015).

et al., 2013; Bridgestock et al., 2016). Furthermore, a comparison of particulate and total Pb concentrations, suggest very low dissolved Pb contents of <5 pmol $kg^{-1}$ throughout the water column at this location (Table 1; Fig. 4e), potentially due to efficient scavenging of Pb by the high suspended particulate load. A recent study demonstrated the importance of equilibrium isotope exchange in coastal waters for modifying the isotope composition of dissolved Pb (Chen et al., 2016). The high particulate concentrations observed in waters of the continental shelf and slope, create conditions conducive to such processes (Fig. 5). Further studies into the distribution of Pb isotope compositions in dissolved and particulate phases are required to fully constrain the impact of such reactions on shelf waters.

### 5.3. Unraveling the sources and cycling of Pb in the eastern Tropical Atlantic

In the following, the observed oceanic distributions of Pb concentrations and isotope compositions are discussed in terms of the transfer of historic anthropogenic Pb emissions into the ocean interior. The distinct Pb isotope compositions and concentrations of the different water masses suggest that ocean circulation is an important mechanism for transfer of anthropogenic Pb into the interior of the Atlantic, in agreement with previous interpretations (Véron et al., 1999; Alleman et al., 1999, 2001; Noble et al., 2015). However, vertical transport of Pb via sinking particles through aggregation/disaggregation and chemical equilibrium processes may also play a role and cannot be completely ruled out (Sherrell and Boyle, 1992; Wu et al., 2010; Chen et al., 2016; Zurbrick et al., 2017).

Due to the short residence time of Pb in the atmosphere (several days; Raes et al., 2000), and the heterogeneous distribution of emission sources, the history of anthropogenic Pb fluxes to ocean surface waters has been significantly different in the northern and southern hemispheres (Kelly et al., 2009; McConnell et al., 2014). We therefore discuss the observed Pb concentrations and isotope compositions of water masses ventilated in the northern and southern hemispheres separately. Through comparison to historic records of anthropogenic Pb emissions, and independent constraints on ventilation timescales, we attempt to unravel the controls on the observed distribution of Pb in the open ocean transect.

#### 5.3.1. Southern hemispheric water masses

South Atlantic Central Water and AAIW are formed by subduction of surface waters within the Antarctic Circumpolar Current, north of the Polar Front, with the more northerly less dense variety contributing to SACW (Stramma and England, 1999). Although no direct historic records of Pb inputs to surface waters, such as reconstructions from coral archives and/or time series measurements of surface waters (e.g. Kelly et al., 2009) exist for this region, ice cores and firn samples provide information on the past delivery of anthropogenic Pb to Antarctica (Rosman et al., 1994; Barbante et al., 1997; Planchon et al., 2003; Vallelonga et al., 2002; Van de Velde et al., 2005; McConnell et al., 2014). Such records are generally consistent across the continent suggesting that they are representative of the Antarctic region, and potentially the southern hemisphere, as a whole and not subject to significant local bias (McConnell et al., 2014).

Two major periods of southern hemispheric anthropogenic Pb depositions are identified in the Antarctic ice core/firn records. For the period between about 1890 and 1910, enrichments of anthropogenic Pb are attributed to metal smelting in Australia (Vallelonga et al., 2002; Van de Velde et al., 2005; McConnell et al., 2014). Following a period of reduced anthropogenic Pb fluxes (~1930 to 1950), they increased to a maximum in the 1970s before declining again, due to the increased usage and subsequent phasing out of leaded petrol in southern hemisphere countries (Planchon et al., 2003; Vallelonga et al., 2002; Van de Velde et al., 2005; McConnell et al., 2014). The $^{206}Pb/^{207}Pb$ ratios associated with the anthropogenic fluxes are lower, at ~1.10–1.20, compared to the pre-anthropogenic background of ~1.20–1.25 (Planchon et al., 2003; Vallelonga et al., 2002; Van de Velde et al., 2005; McConnell et al., 2014). The low $^{206}Pb/^{207}Pb$ ratios of SACW and AAIW at station 12 (1.1566–1.1621) are therefore consistent with anthropogenic southern hemisphere Pb emissions during the past century (Fig. 6a).

A transit time distribution model of CFC and $SF_6$ data yields mean ventilation ages of ~150 years and ~300 years at neutral density horizons corresponding to SACW ($\sigma_\theta = 27.1$) and AAIW ($\sigma_\theta = 27.3$), respectively, for water along the equator of the eastern Tropical Atlantic, close to the position of station 12 (Schneider et al., 2012). These mean ventilation ages pre-date the onset of the anthropogenic Pb perturbation in the southern hemisphere and seem in contrast with the above presented observation of anthropogenic Pb at similar neutral density horizons ($\sigma_\theta = 27.0$ & 27.2) in the Tropical Atlantic Ocean. This discrepancy could result from the vertical transport of anthropogenic Pb into the ocean interior via sinking particles similar to the scenario proposed to explain the presence of anthropogenic Pb in the deep Pacific Ocean (Wu et al., 2010; Zurbrick et al., 2017). In this case, anthropogenic Pb is scavenged from surface waters and transported into the ocean interior by sinking particles, which then undergo equilibrium exchange with dissolved Pb, altering the isotope composition of these waters.

Alternatively we propose that mixing between small amounts of waters with high concentrations of anthropogenic Pb that were ventilated during the past century and older waters that feature much lower quantities of pre-anthropogenic Pb, could feasibly explain the anthropogenic Pb isotope signatures of these water masses. Such mixing of waters with distinct 'ages' and large differences in Pb concentrations would act to dilute the Pb content of the recently ventilated waters without significantly altering their isotope composition. Antarctic ice and firn records indicate that anthropogenic Pb was enriched by a factor of about 70 over the pre-anthropogenic background during the past century (McConnell et al., 2014). A conceptual example of mixing between recently ventilated water enriched in anthropogenic Pb, and much 'older' water, ventilated prior to the onset of anthropogenic emissions is shown in Fig. 7. Here it is assumed that the recently ventilated water has a Pb concentration 70 times higher than the 'older' pre-anthropogenic water, and that these two respective water masses have $^{206}Pb/^{207}Pb$ ratios of 1.16 and 1.21. Notably, the Pb isotope composition of the mixture convergences to those determined for SACW and AAIW in the Tropical Atlantic with only a 20% contribution from the recently ventilated endmember. The approximate factor of 2 lower Pb concentration of AAIW relative to SACW is therefore consistent with the older mean ventilation age of the former (~300 and 150 years for AAIW and SACW respectively), resulting in greater dilution of recently ventilated water with older, 'pre-anthropogenic' water. The exact importance of particulate exchange processes and mixing for setting the observed distribution of

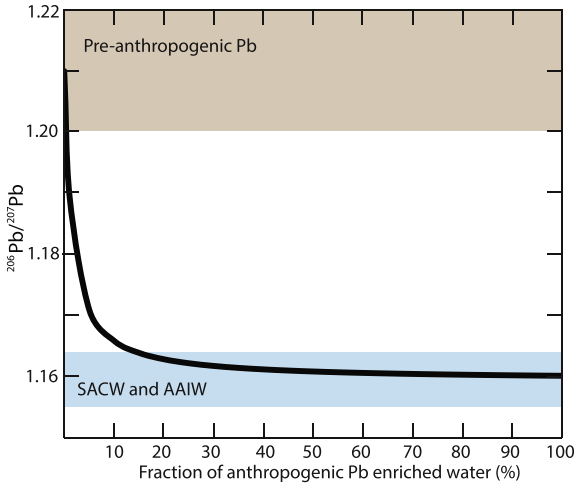


Fig. 7. Conceptual mixing relationship between seawater ventilated in the southern hemisphere during the past century that is enriched in anthropogenic Pb, and 'older' seawater ventilated prior to the onset of significant anthropogenic Pb emissions. The recently ventilated endmember is assumed to have a $^{206}Pb/^{207}Pb$ ratio of 1.16 and 70 times more Pb than the pre-anthropogenic endmember, which features a $^{206}Pb/^{207}Pb$ ratio of 1.21. Colored fields show the range of $^{206}Pb/^{207}Pb$ ratios for pre-anthropogenic southern hemispheric Pb inferred from Antarctic ice cores (Vallelonga et al., 2002; Van de Velde et al., 2005), and $^{206}Pb/^{207}Pb$ ratios determined for South Atlantic Central Water (SACW) and Antarctic Intermediate Water (AAIW) in the Tropical Atlantic (this study). Due to the large difference in Pb concentrations, the Pb isotope composition of the resulting mixture of waters convergences to the $^{206}Pb/^{207}Pb$ ratios determined for SACW and AAIW with only 20% contribution from the recently ventilated endmember.

anthropogenic Pb in these waters remains unclear, but the above analysis highlights the need to consider such mixing scenarios when interpreting distributions of Pb in the ocean interior.

Antarctic bottom water is formed by the subduction of surface waters close to the Antarctic margin, notably in the Weddell and Ross Seas, with additional entrainment of Circumpolar Deep Water (Mantyla and Reid, 1983; Orsi et al., 1999, 2002). This water mass is therefore likely to contain relatively small proportions of recently ventilated water affected by anthropogenic inputs, in accordance with our results for a single sample collected within AABW (station 12, 4500 m water depth). This sample features a low Pb concentration of 7.5 pmol $kg^{-1}$ with an isotope composition that plots towards the pre-anthropogenic background in $^{206}Pb/^{207}Pb$ versus $^{208}Pb/^{207}Pb$ space and which is hence distinct from the lower ratios shown by SACW and AAIW (Figs. 4 and 6). It should, however, be noted that AABW and NADW have almost identical Pb isotope ratios at station 12, indicative of dilution of the original AABW signature by mixing with NADW (Fig. 4). In addition, it is conceivable that the Pb signature of the AABW sample might be significantly influenced by the particulate phase, which contributes 24% to the Pb content of the analyzed sample. The Pb isotope composition determined for AABW sampled in the South Atlantic (Paul et al., 2015b) is, however, similar to that observed here for the Tropical Atlantic Ocean, suggesting that local contributions from particulate phases and/or mixing with NADW may not ply a significant role in setting the observed isotope composition of this water mass.

### 5.3.2. Northern hemispheric water masses

Emissions from North America and Europe have dominated the input of Pb into the North Atlantic during the past century (Wu and Boyle, 1997; Kelly et al., 2009). In detail, coral based reconstructions of the Pb concentrations and isotope compositions of Sargasso Sea surface water for the past 2 centuries are available to aid interpretation of our seawater data (Shen and Boyle, 1987; Desenfant et al., 2006; Kelly et al., 2009). These records are from Bermuda, situated far from the deep water formation sites at high latitudes in the North Atlantic and are likely biased towards North American inputs. However, since US Pb emissions far exceeded European emissions between the 1940s and the 1980s, these records likely provide a reasonable estimate for the composition of waters that were exported from the North Atlantic during this period (Wu and Boyle, 1997; Weiss et al., 2003).

As argued above (Section 5.3.1), mixing of waters ventilated at different times will produce a Pb isotope composition that is biased towards the water with the highest Pb concentration. The highest Pb inputs to the North Atlantic were in the 1970s during peak use of leaded petrol in the surrounding regions, similar to the southern hemispheric records (Shen and Boyle, 1987; Desenfant et al., 2006; Kelly et al., 2009). Hence, transit time estimates based on the Pb isotope compositions of northern sourced waters may be biased towards water mass components that were ventilated during or close to the 1970s. A comparison of our Pb isotope data with those from the coral-based reconstruction of Kelly et al. (2009), show that the signature of our NADW samples, of $^{206}Pb/^{207}Pb = 1.1762$ to 1.1841 and $^{206}Pb/^{207}Pb = 2.4482$ to 2.4571, best matches the Pb emissions during the 1910s to 1930s (Fig. 6). A similar signature was detected by Noble et al. (2015) in NADW collected in the eastern Atlantic in 2011, and suggests a transit time of approximately 80–100 years for at least the most recently ventilated components of this water mass. Schlitzer et al. (1985) used radioactive $^{14}C$ and $^{39}Ar$ to estimate a transit time of ~100–200 years for northern hemisphere derived waters from below 3000 m in the eastern Atlantic, in broad agreement with our interpretation.

The Pb concentration maximum at 600–900 m ($\sigma_\theta = 27.2$–27.4) at station 20 has a Pb isotope composition that matches Sargasso Sea Pb inputs during the 1950s to 1960s, and is similar to the isotope composition of the peak Pb inputs from the 1970s (Fig. 6). We interpret this Pb signature to originate from waters subducted in the Labrador and/or Irminger Seas with a transit time of about 50–60 years. Noble et al. (2015) found Pb concentration maxima at intermediate water depths in the center of the subtropical gyre that were associated with similar Pb isotope compositions and $SF_6$ ventilation ages of ~40 years, consistent with this interpretation. They also found a Pb concentration maximum along the east of the basin (18–23°W) that was

associated with MOW and featured a similar isotope composition (Noble et al., 2015). Based on the location of station 20 (28°W), the Pb concentration maximum is most likely related to that observed by Noble et al. (2015) in the centre of the subtropical gyre. However, MOW may also contribute some Pb to this signature, highlighting the complexity of advective Pb sources to this region at intermediate depths.

The anomalously high concentrations of Pb observed at station 12, between 2500 m and 3700 m water depth, located above the Mid Atlantic Ridge could be due to hydrothermal inputs. However, previous studies have shown that Pb is rapidly removed from vent fluids upon mixing with seawater, by co-precipitation with and scavenging by sulphides (Le Hurray et al., 1988; Godfrey et al., 1994; Noble et al., 2015), so that elevated seawater Pb concentrations due to hydrothermal activity are not expected. In this context, it cannot be completely ruled out that the observed maximum in Pb concentration is due to contamination during sample collection and handling. Furthermore, hydrothermally derived Pb is expected to have an isotope composition similar to that of mid ocean ridge basalts (Le Hurray et al., 1988; Godfrey et al., 1994), which differ significantly ($^{206}Pb/^{207}Pb$ = 1.121–1.125, $^{208}Pb/^{207}Pb$ = 2.461–2.456; Ito et al., 1987) at this location from ambient seawater ($^{206}Pb/^{207}Pb$ = 1.17–1.18, $^{208}Pb/^{207}Pb$ = 2.45). The lack of variation in Pb isotope compositions across this depth range at station 12 is therefore at odds with any hydrothermal inputs of Pb at this location, but could reflect mobilization of Pb from sediments by hydrothermal fluids, which are known to feature a range of Pb isotope compositions that encompass the values determined for the seawater at this location (Hamelin et al., 1990).

*5.3.3. Mixing of historic northern and southern hemispheric Pb emissions*

The Tropical Atlantic features a complex circulation regime. At intermediate to shallow depths (<1000 m) a series of alternating zonal currents transport and mix waters ventilated in the northern and southern hemispheres (Stramma and Schott, 1999). The location, depth, magnitude and even direction of these currents can vary over short timescales and can be difficult to predict (Schott et al., 2003; Stramma et al., 2005; Brandt et al., 2008). Given the differences in Pb isotope composition between Atlantic water masses derived from the northern and southern hemisphere, Pb isotopes may prove a useful tracer of water mass mixing in this hydrographically complex region. To this end, samples collected at <1000 m depth at station 16 are interpreted in the following in terms of mixing of waters sampled at stations 20 and 12, representing ISW/LSW and AAIW respectively. In particular, this exercise focuses on samples collected at each of these stations along the neutral density horizon $\sigma_\theta = 27.3–27.4$, in 600 to 800 m water depth (Fig. 4).

Antarctic Intermediate Water enters the Tropical Atlantic via the Intermediate Western Boundary Current off the northeast coast of Brazil (Stramma and Schott, 1999). Likewise, northern sourced water masses enter the region via the Deep Western Boundary Current (Stramma and Schott, 1999). The western Tropical Atlantic is therefore an important region for the mixing of northern and southern sourced water masses. These waters are then transported into the eastern basin via a series of zonal currents. In particular, a northern branch of the eastward flowing North Equatorial Countercurrent that extends down into AAIW, has been identified at 8–10°N coinciding with the position of station 16 (Stramma et al., 2005).

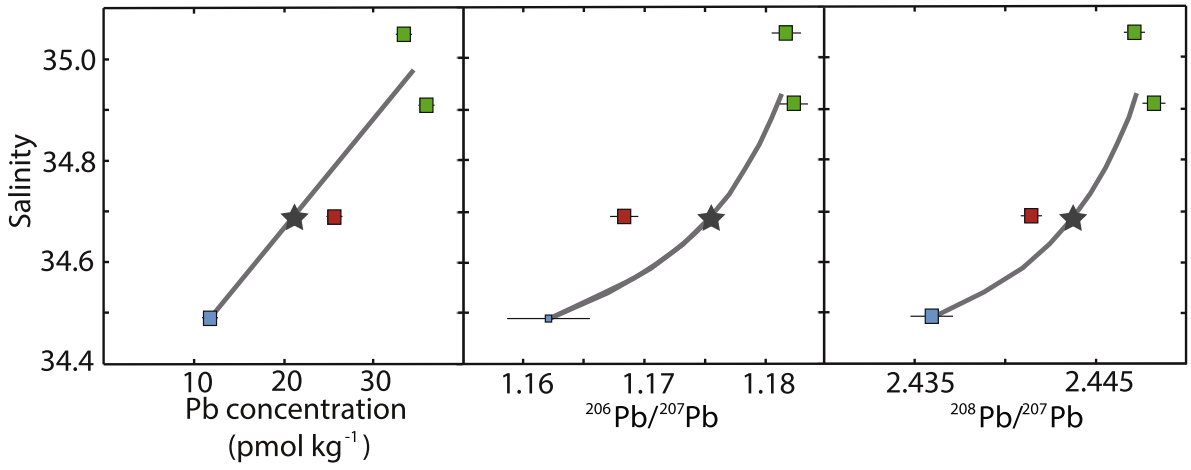


Fig. 8. Plots of salinity versus total Pb concentration, $^{206}Pb/^{207}Pb$ and $^{208}Pb/^{207}Pb$ ratios for seawater samples collected along the $\sigma_\theta = 27.3–27.4$ neutral density horizon relevant for the core of AAIW and mixing with more saline northern sourced waters. Grey lines show idealized mixing lines between endmember compositions from station 12 (blue symbol; AAIW) and 20 (green symbols; LSW/ISW/MOW) at the same neutral density horizon. Grey stars denote the compositions predicted for station 16 assuming two component mixing between AAIW (station 12) and LSW/ISW/MOW (station 20). The red square shows the measured compositions for seawater at station 16, highlighting that water mass mixing alone is unable to account for the observed seawater Pb signature. (For interpretation of the references to colour in this figure legend, the reader is referred to the web version of this article.)

Based on salinity, intermediate water from 750 m depth at station 16 is a 6+4 mixture of waters from stations 12 and 20. Taking the samples from station 12 at 750 m and station 20 at 899 m as endmembers (Table 1), a mass balance calculation predicts that the water mixture at station 16, 750 m should be characterized by [Pb] = 20.9 pmol $kg^{-1}$, $^{206}Pb/^{207}Pb = 1.1753$ and $^{208}Pb/^{207}Pb = 2.4437$. Compared to the actual observations, with [Pb] = 25.7 pmol $kg^{-1}$, $^{206}Pb/^{207}Pb = 1.1683$ and $^{208}Pb/^{207}Pb = 2.4415$, the calculated Pb concentration is too low and the predicted $^{206}Pb/^{207}Pb$ and $^{208}Pb/^{207}Pb$ ratios are too high (Fig. 8). This discrepancy likely reflects the transient evolution of the Pb concentration and isotope composition of the endmember water masses, reflecting the non-steady state distribution of Pb in this region of the ocean. Constraints on the distribution of Pb concentrations and isotope compositions in the western Tropical Atlantic may allow further insights into the complex mixing dynamics of anthropogenic Pb in this region.

## 6. CONCLUSIONS

The use of high-precision Pb isotope data that includes the minor non-radiogenic isotope $^{204}Pb$ does not provide additional information on Pb sources to Tropical Atlantic seawater compared to isotopic data which features solely the radiogenic isotopes $^{206}Pb$, $^{207}Pb$ and $^{208}Pb$. This finding most likely reflects the particular isotope systematics of the most important Pb ore bodies that have been exploited for production and which have been the dominant sources of Pb to the environment in recent history. The commonly followed approach of neglecting Pb isotope ratios featuring $^{204}Pb$ for source apportionment is therefore justified.

The distributions of Pb concentrations and isotope compositions in the interior of the eastern Tropical Atlantic are related to hydrographic variations, and are generally consistent with those expected for the penetration of transient anthropogenic Pb inputs via ocean circulation. This is particularly apparent for water masses ventilated in the northern hemisphere, in which Pb concentrations and isotope composition variations are consistent with those expected based on differences in ventilation timescales, supporting the notion that the transfer of anthropogenic Pb into the ocean interior can provide useful insights into ventilation pathways and timescales.

Mixing of waters ventilated at different times that feature large differences in Pb concentrations in addition to particulate exchange processes, can however complicate straightforward interpretation of Pb concentration and isotope composition distributions in the ocean in terms of ventilation timescales. This is particularly evident for the southern hemisphere water masses SACW and AAIW, which feature anthropogenic Pb isotope compositions even though independent tracers are indicative of ventilation ages that pre-date the onset of significant anthropogenic Pb emissions in the southern hemisphere (Schneider et al., 2012). With increasing data coverage, future modeling studies may help unravel the complex interplay between transient inputs, advection, mixing and chemical reactivity in producing the observed distribution of Pb in the ocean.

## ACKNOWLEDGEMENTS

We thank the captain, crew and cruise participants of the RRS *Discovery* during the D361 cruise (GEOTRACES section GA06). Katharina Kreissig and Barry Coles are thanked for keeping the MAGIC clean labs and mass spectrometer running, and the MAGIC research group for their support and guidance. The authors acknowledge funding from the following NERC grants: L.B., T. v.d.F. and M.R. by NE/J021636/1 and NE/H005390/1; M.L by NE/G016267/1 and EPA by NE/G015732/1. Conflicts of interest: none.

## AUTHOR CONTRIBUTIONS

L.B., T.v.d.F. and M.R conceived the study, and L.B conducted all Pb concentration and isotope analyses of unfiltered seawater with assistance from M.P. Measurements of particulate Pb concentrations were conducted by A.M and M.C.L. The collection of the unfiltered seawater and particulate samples was conducted by M.C.L, A.M. and E.P.A. The manuscript was written by L.B with inputs from all co-authors.

## APPENDIX A. SUPPLEMENTARY MATERIAL

Supplementary data associated with this article can be found, in the online version, at https://doi.org/10.1016/j.gca.2018.01.018.

## REFERENCES

Abouchami W., Nathe K., Kumar A., Galer S. J. G., Jochum K. P., Williams E. and Andreae M. O. (2013) Geochemical and isotopic characterization of the Bodele Depression dust source and implications for transatlantic dust transport to the Amazon Basin. *Earth Planet. Sci. Lett.* **380**, 112–123.

Abouchami W. and Zabel M. (2003) Climate forcing of the Pb isotope record of terrigenous input into the Equatorial Atlantic. *Earth Planet. Sci. Lett.* **213**(3–4), 221–234.

Alleman L. Y., Véron A. J., Church T. M., Flegal A. R. and Hamelin B. (1999) Invasion of the abyssal North Atlantic by modern anthropogenic lead. *Geophys. Res. Lett.* **26**(10), 1477–1480.

Alleman L. Y., Church T. M., Ganguli P., Véron A. J., Hamelin B. and Flegal A. R. (2001) Role of oceanic circulation on contaminant lead distribution in the South Atlantic. *Deep-Sea Res. II* **48**(13), 2855–2876.

Barbante C., Turetta C., Capodaglio G. and Scarponi G. (1997) Recent decrease in the lead concentration of Antarctic snow. *Int. J. Environ. Anal. Chem.* **68**(4), 457–477.

Bollhöfer A. and Rosman K. J. R. (2001) Isotopic source signatures for atmospheric lead: the Northern Hemisphere. *Geochim. Cosmochim. Acta* **65**(11), 1727–1740.

Boyle E. A., Chapnick S. D., Shen G. T. and Bacon M. P. (1986) Temporal variability of lead in the western North-Atlantic. *Journal of Geophysical Research-Oceans* **91**(C7), 8573–8593.

Boyle E. A., John S., Abouchami W., Adkins J. F., Echegoyen-Sanz Y., Ellwood M. and Zhao Y. (2012) GEOTRACES IC1 (BATS) contamination-prone trace element isotopes Cd, Fe, Pb, Zn, Cu, and Mo intercalibration. *Limnol. Oceanogr.-Methods* **10**, 653–665.

Boyle E. A., Lee J. M., Echegoyen Y., Noble A., Moos S., Carrasco G. and Norisuye K. (2014) Anthropogenic lead emission in the ocean the evolving global experiment. *Oceanography* **27**(1), 69–75.

Brandt P., Hormann V., Bourles B., Fischer J., Schott F. A., Stramma L. and Dengler M. (2008) Oxygen tongues and zonal currents in the equatorial Atlantic. *J. Geophys. Res.-Oceans* **113** (C4).

Bridgestock L., van de Flierdt T., Rehkämper M., Paul M., Middag R., Milne A., Maeve L. C., Baker A. R., Chance R., Khondoker R., Strekopytov S., Humphrey-Williams E., Achterberg E. P., Rijkenberg M. J. A., Gerrringa L. J. A. and de Baar H. J. W. (2016) Return of naturally sourced Pb to Atlantic surface waters. *Nat. Commun.* **7**, 12921. https://doi.org/10.1038/NCOMMS12921.

Chen M., Boyle E. A., Lee J.-M., Nurhati I., Zurbrick C., Switzer A. D. and Gonzalo C. (2016) Lead isotope exchange between dissolved and fluvial particulate matter: a laboratory study from the Johor River estuary. *Philosoph. Transact. A* **374**, 20160054. https://doi.org/10.1098/rsta.2016.0054.

Chow T. J. and Patterson C. C. (1962) The occurrence and significance of lead isotopes in pelagic sediments. *Geochim. Cosmochim. Acta* **26**(2), 263–308.

Chow T. J. and Patterson C. C. (1966) Concentration profiles of barium and lead in Atlantic waters off Bermuda. *Earth Planet. Sci. Lett.* **1**, 397–400.

Desenfant F., Véron A. J., Camoin G. F. and Nyberg J. (2006) Reconstruction of pollutant lead invasion into the tropical North Atlantic during the twentieth century. *Coral Reefs* **25**(3), 473–484. https://doi.org/10.1007/s00338-006-0113-x.

Doney S. C., Jenkins W. J. and Bullister J. L. (1997) A comparison of ocean tracer dating techniques on a meridional section in the eastern North Atlantic. *Deep-Sea Res. I* **44**(4), 603–626. https://doi.org/10.1016/S0967-0637(96)00105-7.

Emery W. J. and Meincke J. (1986) Global water masses – summary and review. *Oceanol. Acta* **9**(4), 383–391.

Fine R. A. (2011) Observations of CFCs and $SF_6$ as ocean tracers. *Annu. Rev. Mar. Sci.* **3**, 173–195. https://doi.org/10.1146/annurev.marine.010908.163933.

Godfrey L. V., Mills R., Elderfield H. and Gurvich E. (1994) Lead behavior at the tag hydrothermal vent field, 26°N, mid-atlantic ridge. *Mar. Chem.* **46**(3), 237–254. https://doi.org/10.1016/0304-4203(94)90080-9.

Hamelin B., Grousset F. and Sholkovitz E. R. (1990) Pb Isotopes in surficial pelagic sediments from the North Atlantic. *Geochim. Cosmochim. Acta* **54**(1), 37–47. https://doi.org/10.1016/0016-7037(90)90193-O.

Hamelin B., Ferrand J. L., Alleman L., Nicolas E. and Véron A. (1997) Isotopic evidence of pollutant lead transport from North America to the subtropical North Atlantic gyre. *Geochim. Cosmochim. Acta* **61**(20), 4423–4428. https://doi.org/10.1016/S0016-7037(97)00242-1.

Hurst R. W. (2002) Lead isotopes as age-sensitive genetic markers in hydrocarbons. 3. Leaded Gasoline, 1923–1990 (ALAS Model). *Environ. Geosci.* **9**(2), 43–50. https://doi.org/10.1046/j.1526-0984.2002.92003.x.

Ito E., White W. M. and Gopel C. (1987) The O, Sr, Nd and Pb Isotope Geochemistry of MORB. *Chem. Geol.* **62**(3–4), 157–176. https://doi.org/10.1016/0009-2541(87)90083-0.

Jenkins W. J., Smethie W. M., Boyle E. A. and Cutter G. A. (2015) Water mass analysis for the US GEOTRACES (GA03) North Atlantic sections. *Deep-Sea Res. II* **116**, 6–20. https://doi.org/10.1016/j.dsr2.2014.11.018.

Kelly A. E., Reuer M. K., Goodkin N. F. and Boyle E. A. (2009) Lead concentrations and isotopes in corals and water near Bermuda, 1780–2000. *Earth Planet. Sci. Lett.* **283**, 93–100. https://doi.org/10.1016/J.Epsl. 2009.03.045.

Komárek M., Ettler V., Chrastny V. and Mihaljevic M. (2008) Lead isotopes in environmental sciences: a review. *Environ. Int.* **34**(4), 562–577. https://doi.org/10.1016/j.envint.2007.10.005.

Lee J.-M., Boyle E. A., Echegoyen-Sanz Y., Fitzsimmons J. N., Zhang R. F. and Kayser R. A. (2011) Analysis of trace metals (Cu, Cd, Pb, and Fe) in seawater using single batch nitrilotriacetate resin extraction and isotope dilution inductively coupled plasma mass spectrometry. *Anal. Chim. Acta* **686**(1–2), 93–101. https://doi.org/10.1016/j.aca.2010.11.052.

Lee J.-M., Eltgroth S. F., Boyle E. A. and Adkins J. F. (2017) The transfer of bomb radiocarbon and anthropogenic lead to the deep North Atlantic Ocean observed from a deep sea coral. *Earth Planet. Sci. Lett.* **458**, 223–232. https://doi.org/10.1016/j.epsl.2016.10.049.

Le Hurray A. P., Church S. E., Koski R. A. and Bouse R. M. (1988) Pb isotopes in sulfides from mid-ocean ridge hydrothermal sites. *Geology* **16**(4), 362–365.

Mantyla A. W. and Reid J. L. (1983) Abyssal characteristics of the world ocean waters. *Deep-Sea Res.* **30**(8), 805–833. https://doi.org/10.1016/0198-0149(83)90002-X.

Mawji et al. (2015) The GEOTRACES intermediate data product 2014. *Mar. Chem.* **177**(1), 1–8. https://doi.org/10.1016/j.marchem.2015.04.005.

McConnell J. R., Maselli O. J., Sigl M., Vallelonga P., Neumann T., Anschutz H. and Thomas E. R. (2014) Antarctic-wide array of high-resolution ice core records reveals pervasive lead pollution began in 1889 and persists today. *Sci. Rep.* **4**, 5848. https://doi.org/10.1038/srep05848.

Noble A. E., Echegoyen-Sanz Y., Boyle E. A., Ohnemus D. C., Lam P. J., Kayser R. and Smethie W. (2015) Dynamic variability of dissolved Pb and Pb isotope composition from the US North Atlantic GEOTRACES transect. *Deep-Sea Res. II* **116**, 208–225. https://doi.org/10.1016/j.dsr2.2014.11.011.

Nriagu J. O. and Pacyna J. M. (1988) Quantitative assessment of worldwide contamination of air, water and soils by trace-metals. *Nature* **333**(6169), 134–139. https://doi.org/10.1038/333134a0.

O'Connor B. M., Fine R. A. and Olson D. B. (2005) A global comparison of subtropical underwater formation rates. *Deep-Sea Res. I* **52**(9), 1569–1590. https://doi.org/10.1016/j.dsr.2005.01.011.

Ohnemus D. C., Auro M. E., Sherrell R. M., Lagerström M., Morton P. L., Twining B. S., Rauschenberg S. and Lam P. J. (2014) Laboratory intercomparison of marine particulate digestions including Piranha: a novel chemical method for dissolution of polyethersulfone filters. *Liminol. Oceanogr.: Methods* **12**, 530–547. https://doi.org/10.4319/lom.2014.12.530.

Orsi A. H., Johnson G. C. and Bullister J. L. (1999) Circulation, mixing, and production of Antarctic Bottom Water. *Prog. Oceanogr.* **43**(1), 55–109. https://doi.org/10.1016/S0079-6611(99)00004-X.

Orsi A. H., Smethie W. M. and Bullister J. L. (2002) On the total input of Antarctic waters to the deep ocean: a preliminary estimate from chlorofluorocarbon measurements. *J. Geophys. Res.-Oceans* **107**(C8). https://doi.org/10.1029/2001jc000976.

Pacyna J. M. and Pacyna E. G. (2001) An assessment of global and regional emissions of trace metals to the atmosphere from anthropogenic sources worldwide. *Environ. Rev.* **9**(4), 296–298.

Paul M., van de Flierdt T., Rehkämper M., Khondoker R., Weiss D., Lohan M. C. and Homoky W. B. (2015a) Tracing the Agulhas leakage with lead isotopes. *Geophys. Res. Lett.*. https://doi.org/10.1002/2015GL065625.

Paul M., Bridgestock L., Rehkämper M., van de Flierdt T. and Weiss D. (2015b) High-precision measurements of seawater Pb

isotope compositions by double spike thermal ionization mass spectrometry. *Anal. Chimica Acta* **863**, 59–69. https://doi.org/10.1016/j.aca.2014.12.012.

Planchon F. A. M., van de Velde K., Rosman K. J. R., Wolff E. W., Ferrari C. P. and Boutron C. F. (2003) One hundred fifty-year record of lead isotopes in Antarctic snow from Coats Land. *Geochim. Cosmochim. Acta* **67**(4), 693–708. https://doi.org/10.1016/S0016-7037(00)01136-5.

Raes F., Van Dingenen R., Vignati E., Wilson J., Putaud J. P., Seinfeld J. H. and Adams P. (2000) Formation and cycling of aerosols in the global troposphere. *Atmos. Environ.* **34**(25), 4215–4240. https://doi.org/10.1016/S1352-2310(00)00239-9.

Rosman K. J. R., Chisholm W., Boutron C. F., Candelone J. P. and Patterson C. C. (1994) Anthropogenic lead isotopes in Antarctica. *Geophys. Res. Lett.* **21**(24), 2669–2672. https://doi.org/10.1029/94gl02603.

Sangster D. F., Outridge P. M. and Davis W. J. (2000) Stable lead isotope characteristics of lead ore deposits of environmental significance. *Environ. Rev.* **8**(2), 115–147.

Schaule B. K. and Patterson C. C. (1983) Perturbations of the natural lead depth profile in the Sargasso Sea by industrial lead. In *Trace Metals in Sea Water* (eds. C. S. Wong, E. A. Boyle, K. W. Bruland, J. D. Burton and E. D. Goldberg). Springer, US, pp. 487–503.

Schlitzer R. (1987) Renewal rates of east-atlantic deep-water estimated by inversion of $^{14}C$ data. *J. Geophys. Res.-Oceans* **92**, 2953–2969. https://doi.org/10.1029/Jc092ic03p02953.

Schlitzer, R., 2015. Ocean Data View, <http://odv.awi.de>.

Schlitzer R., Roether W., Weidmann U., Kalt P. and Loosli H. H. (1985) A meridional $^{14}C$ and $^{39}Ar$ section in Northeast Atlantic Deep-Water. *J. Geophys. Res.-Oceans* **90**, 6945–6952. https://doi.org/10.1029/Jc090ic04p06945.

Schneider A., Tanhua T., Kortzinger A. and Wallace D. W. R. (2012) An evaluation of tracer fields and anthropogenic carbon in the equatorial and the tropical North Atlantic. *Deep-Sea Res. I* **67**, 85–97. https://doi.org/10.1016/j.dsr.2012.05.007.

Schott F. A., Dengler M., Brandt P., Affler K., Fischer J., Bourles B. and Rhein M. (2003) The zonal currents and transports at 35°W in the tropical Atlantic. *Geophys. Res. Lett.* **30**(7). https://doi.org/10.1029/2002gl016849.

Shen G. T. and Boyle E. A. (1987) Lead in corals – reconstruction of historical industrial fluxes to the surface ocean. *Earth Planet. Sci. Lett.* **82**(3–4), 289–304. https://doi.org/10.1016/0012-821x(87)90203-2.

Shen G. T. and Boyle E. A. (1988) Thermocline ventilation of anthropogenic lead in the Western North-Atlantic. *J. Geophys. Res.-Oceans* **93**(C12), 15715–15732. https://doi.org/10.1029/Jc093ic12p15715.

Sherrell R. M. and Boyle E. A. (1992) Isotopic equilibration between dissolved and suspended particulate lead in the atlantic-ocean – evidence from $^{210}Pb$ and Stable Pb Isotopes. *J. Geophys. Res.-Oceans* **97**(C7), 11257–11268. https://doi.org/10.1029/92jc00759.

Stacey J. S. and Kramers J. D. (1975) Approximation of terrestrial lead isotope evolution by a two-stage model. *Earth Planet. Sci. Lett.* **26**, 207–221.

Stramma L. and England M. H. (1999) On the water masses and mean circulation of the South Atlantic Ocean. *J. Geophys. Res.-Oceans* **104**(C9), 20863–20883, 0.1029/1999jc900139.

Stramma L., Huttl S. and Schafstall J. (2005) Water masses and currents in the upper tropical northeast Atlantic off northwest Africa. *J. Geophys. Res.-Oceans* **110**(C12). https://doi.org/10.1029/2005jc002939.

Stramma L. and Schott F. (1999) The mean flow field of the tropical Atlantic Ocean. *Deep-Sea Res. Part II* **46**(1–2), 279–303. https://doi.org/10.1016/S0967-0645(98)00109-X.

Tsuchiya M., Talley, L.D. and McCartney M.S., (1992). An eastern Atlantic section from Iceland southward across the equator, Deep-Sea Res. 39, 1885-1917.

Vallelonga P., Van de Velde K., Candelone J. P., Morgan V. I., Boutron C. F. and Rosman K. J. R. (2002) The lead pollution history of Law Dome, Antarctica, from isotopic measurements on ice cores: 1500 AD to 1989 AD. *Earth Planet. Sci. Lett.* **204** (1–2), 291–306.

Van de Velde K., Vallelonga P., Candelone J. P., Rosman K. J. R., Gaspari V., Cozzi G. and Boutron C. F. (2005) Pb isotope record over one century in snow from Victoria Land, Antarctica. *Earth Planet. Sci. Lett.* **232**(1–2), 95–108. https://doi.org/10.1016/j.epsl.2005.01.007.

Véron A. J., Church T. M., Flegal A. R., Patterson C. C. and Erel Y. (1993) Response of lead cycling in the surface Sargasso Sea to changes in tropospheric input. *J. Geophys. Res.-Oceans* **98** (C10), 18269–18276. https://doi.org/10.1029/93jc01639.

Véron A. J., Church T. M., Patterson C. C. and Flegal A. R. (1994) Use of stable lead isotopes to characterize the sources of anthropogenic lead in North-Atlantic surface waters. *Geochim. Cosmochim. Acta* **58**(15), 3199–3206. https://doi.org/10.1016/0016-7037(94)90047-7.

Véron A. J., Church T. M. and Flegal A. R. (1998) Lead isotopes in the western North Atlantic: transient tracers of pollutant lead inputs. *Environ. Res.* **78**(2), 104–111. https://doi.org/10.1006/Enrs.1998.3856.

Véron A. J., Church T. M., Rivera-Duarte I. and Flegal A. R. (1999) Stable lead isotopic ratios trace thermohaline circulation in the subarctic North Atlantic. *Deep-Sea Res. II* **46**(5), 919–935. https://doi.org/10.1016/S0967-0645(99)00009-0.

Weiss D., Boyle E. A., Wu J. F., Chavagnac V., Michel A. and Reuer M. K. (2003) Spatial and temporal evolution of lead isotope ratios in the North Atlantic Ocean between 1981 and 1989. *J. Geophys. Res.-Oceans* **108**(C10). https://doi.org/10.1029/2000jc000762.

Wu J. F. and Boyle E. A. (1997) Lead in the western North Atlantic Ocean: completed response to leaded gasoline phase-out. *Geochim. Cosmochim. Acta* **61**(15), 3279–3283. https://doi.org/10.1016/S0016-7037(97)89711-6.

Wu J. F., Rember R., Jin M. B., Boyle E. A. and Flegal A. R. (2010) Isotopic evidence for the source of lead in the North Pacific abyssal water. *Geochim. Cosmochim. Acta* **74**(16), 4629–4638. https://doi.org/10.1016/j.gca.2010.05.017.

Zenk W., Klein B. and Schroder M. (1991) Cape-verde frontal zone. *Deep-Sea Res. Part A, Oceanogr. Res. Papers* **38**, S505–S530.

Zurbrick C. M., Gallon C. and Flegal A. R. (2017) Historic and industrial lead within the Northwest Pacific Ocean evidenced by lead isotopes in seawater. *Environ. Sci. Technol.* **51**, 1203–1212. https://doi.org/10.1021/acs.est.6b04666.

## FURTHER READING

Tomczak M., & Godfrey J. S. (1994) Regional Oceanography: an Introduction.

*Associate Editor:* Claire Rollion-Bard